31st Congress of the International Council of the Aeronautical Sciences
Belo Horizonte, Brazil; September 09-14, 2018

SIMULATIONS OF UNSTEADY AIRWAKES BEHIND SHIPS IN MOTION

Weixing Yuan, Alanna Wall, and Richard Lee
National Research Council (NRC) Canada, Ottawa, Ontario, K1A 0R6, Canada
Weixing.Yuan@nrc-cnrc.gc.ca

Keywords: *Unsteady aerodynamics, ship airwakes, computational fluid dynamics (CFD)*

Abstract

To aid pilot training for shipboard helicopter operations, computational fluid dynamics is increasingly being performed to model ship airwakes. Ship motion effects on the airwake could play an important role in affecting pilot workload; however, the level of importance is currently unknown. Work is currently underway to assess ship motion effects on pilot workload, which requires the development of computational tools capable of correctly simulating ship motion.

In the Canadian context, work to expand ship airwake simulation capabilities is currently being done using the open-source OpenFOAM. This paper reports on the progress of this work using airfoils and a real-world Canadian Patrol Frigate, to develop and concept-prove the methodologies for ship-in-motion conditions. Different motion solvers and functions in OpenFOAM are developed or tested for undeforming boundary conditions. The computed results are in reasonably good agreement with the experimental data. Encouraged by promising progress, the capability of using a dynamic mesh is being developed towards application to a real frigate. Assessing the importance of ship motion to pilot workload and the appropriate implementation in flight simulators are the subjects of future work.

1 Introduction

The operation of helicopters from and onto naval ships is a challenging task for pilots. The launch and recovery of a helicopter takes place on a small landing deck located at the stern of a ship, which is subject to multi-degree-of-freedom (multi-DOF) motion in pitch, roll, and heave. The difficulty is increased owing to the fact that the landing deck is immersed in the ship airwake. Because of the nature of bluff-body aerodynamics, the flow separation and sheared vortices interact, resulting in a time-varying airwake with highly turbulent structures, which can significantly intensify the pilot workload and impact precision positioning for helicopter operations.

It is now common to use flight simulation to aid pilot training for shipboard helicopter operations. One of the key areas for improvement is the modelling of ship airwakes. Although at-sea and wind-tunnel measurements can be used to provide data from which airwake models can be generated, computational fluid dynamics (CFD) is being used increasingly to model ship airwakes. With this approach, CFD solves the flow over the ship, and the resulting velocity field data are exported to a flight simulator as look-up tables.

The shipboard environment is highly complex, where factors such as atmospheric boundary layer, variations in wind speed and direction, differences in helicopter hover position, ship draft, and seaways, as well as other factors, result in an airwake with characteristics which vary relative to the idealized airwake simulated in the wind tunnel and CFD. Since operational limits and procedures must inherently account for these realistic variations, the level of agreement for modelling and simulation tools must be, at this time, on the order of 10%, with similar trends and features, to be considered useful for training and other purposes.

Computations have been extensively carried out for an updated version of a simple frigate shape (SFS2), including the work demonstrated in Ref. [1]. After the successful validation of the CFD solver OpenFOAM against the static SFS2 geometry, CFD was applied to the Canadian Patrol Frigate (CPF) with no motion. Details of the computed results of the flows past the static CPF were summarized in Ref. [2]. Having successfully applied the CFD to the static cases, simulations for a ship in motion are now under development.

For flight simulators, the feasibility of implementing real-time CFD, with correctly simulated ship motion, is currently limited. The long-term objective of the work described in this paper, is to assess the relative importance of the ship motion element on the airwake properties for helicopter operations so that the fidelity of flight simulators can be improved to an appropriate level, with or without full computational airwake solutions. This paper covers the development of CFD solutions for representative ship motion conditions and comparisons with wind tunnel data. As the work progresses, further consideration of at-sea data is expected to lead to recommendations for modification of the flight simulators.

Since ship motion effects on the airwake could possibly play an important role when large amplitude ship motions are present [3], the effect of ship motion on the airwake is being investigated at NRC using both computational and experimental simulations. The computational component of this investigation considers delayed detached eddy simulations (DDES) [4] based on the open-source OpenFOAM [5] for the CPF in motion. To evaluate and validate the motion solvers and functions implemented in OpenFOAM, simulations were performed for simple oscillating airfoils and wings. Based on the success of these validations, simulations of flows past the CPF in motion are in progress. The ship motion effects on the airwake are discussed in the paper. The results from computations and experimental measurements for the ship in both static and motion conditions are cross-compared against each other.

2 Description of OpenFOAM

The purpose of this work is to validate the results produced by OpenFOAM [5], the tool of choice for this work, against experimental data and to determine whether OpenFOAM is suitable for ship airwake simulations. OpenFOAM's pimpleFoam is a pressure-based transient Navier-Stokes solver, allowing for relatively large time steps using the hybrid PISO-SIMPLE (PIMPLE) algorithm. The pimpleDyMFoam solver is an implementation of the pimpleFoam solver which allows for dynamic meshes.

OpenFOAM applies the integral form of the conservation laws of mass and momentum on an unstructured grid. A fully-implicit, second-order temporal differencing scheme was implemented in the discretization. The discretization of the convective and diffusive fluxes was carried out in a co-located variable arrangement using a finite-volume approach, which was second-order accurate in space. The linear-upwind stabilized transport (LUST) scheme blends linear-upwind with linear interpolation to stabilize solutions while maintaining second-order behavior. The coupling of the pressure and velocity was handled using a modified SIMPLE algorithm in the PIMPLE computations. Because of the nature of the bluff-body aerodynamics, the Spalart-Allmaras DDES [4] was employed to model the turbulence, unless stated otherwise.

OpenFOAM has several motion functions to define the boundary or body motions. Typically, the oscillating-linear and oscillating-rotating motion functions can be used to define simple sinusoidal translating and rotating motion profiles, respectively. Since these oscillating motion functions do not have parameters for setting phase shift between multiple motions, it cannot be directly used for multi-DOF motions without modifications of the OpenFOAM source code. Alternatively, the tabulated6DOFMotion function allows to pre-generate tabulated motion schedules. As improper round offs may cause numerical instabilities and unphysical solutions, the tabulated motion schedules must be defined in double precision if the time step is small.

OpenFOAM uses motion solvers to calculate the mesh displacement. A basic solid-body motion solver was used in this work; it allows for mesh motion where the mesh topology does not change and the computational mesh moves as a whole. Although it can be used only for simulations without deforming boundaries, it is an effective approach to validate flow solvers, as shown in this study.

OpenFOAM also has some motion solvers for modelling dynamic meshes. Unfortunately, they were developed for some specific conditions and applications. To handle the complex ship motions with deforming free-surface boundary, a mesh morphing functionality was ported from Caelus [6] to OpenFOAM. Caelus is open-source software and a derivative of OpenFOAM. The ported mesh morphing functionality was originally implemented in OpenFOAM by F. Bos and D. Matijasevic based on radial basis functions (RBF) as described in Ref. [7]. As the new functionality is still being tested for ship motions, only 2D solutions of airfoils will be demonstrated in this paper.

3 Validation of Motion Functions against Airfoils in Motion

The motion solvers and functions were validated first against single airfoils in motion. The airfoils considered include a NACA 0012 airfoil oscillating in pitch, a SD7003 airfoil in plunge, and a NACA 0005 airfoil in pitch-plunge motion. The pimpleDyMFoam was chosen as the flow solver. Both the oscillating and tabulated motion functions were used to define the motions of the pitching NACA 0012 and plunging SD7003 airfoils in the simulations. Since the current oscillating motion functions cannot define the phase shift between motions, the tabulated motion function was employed for the pitching-plunging case with a NACA 0005 airfoil. As with previous studies using an in-house code at NRC, the solid-body motion solver was applied to calculate the mesh motion for all the three cases. To demonstrate the potential of the dynamic motion solver, incorporated with the RBFs, the ported mesh morphing functionality was applied to the NACA 0005 airfoil in pitch-plunge motion.

3.1 NACA 0012 Airfoil in Pitch Motion

To evaluate and validate the performance of the aforementioned algorithms, a wing based on a NACA 0012 airfoil, with validation results available in open literature, was chosen as the test case. The wing was rectangular in planform with a chord of 30.48 cm (1 ft) and a span of 60.96 cm (2 ft). Halfman [8] has reported analytical solutions (using vortex-sheet theory) and experimental results for this wing. In the experiment, the wing was subjected to a free stream velocity of $u_\infty = 36$ m/s; it was pitched dynamically about an axis located at 37% of the chord, at a reduced frequency of $k_c = \omega b / u_\infty = 0.4$, where $b=c/2$ is the semi-chord and ω is the angular frequency of the pitching motion. The freestream Mach and Reynolds numbers were 0.11 and 6.9×10^5, respectively. The amplitude of the motion, θ, was equal to 6.74° and centred around $\theta = 0°$.

A previous numerical study employing INSflow [9], an NRC in-house CFD code, was used as a start point to ease the setup with OpenFOAM. An O-H type mesh was used in the calculations. The mesh had 121×40×41 grid points in the chordwise, normal to the wall and spanwise directions, respectively. The outer boundary was ten chords away from the wing. The meshes used in this study were generated using a blunt trailing edge which is representative of the actual model, more so than a sharp trailing edge. Inlet and outlet boundary conditions were set in the current OpenFOAM simulations.

With air as the fluid, the computations were started from a uniform flow set with a freestream velocity of 36 m/s. The period of one oscillation cycle was divided into 96 time steps. In the current OpenFOAM calculations, 20 nonlinear iterations were limited per time step. The calculations of the third pitching cycle reproduced the results of the second pitching cycle. Figure 1 compares the 3rd cycle results against the previous computed [9] and experimental [8] data. As can be seen in the figure, the dynamic performance of the computed oscillating wing, including the time-dependent history of the lift and the pitching moment coefficients, were in close agreement with the experimental data.

3.2 SD7003 Airfoil in Plunge Motion

2D calculations were performed for a SD7003 airfoil at an angle of attack of 8° in a sinusoidal plunge motion. The airfoil had a chord length of 20.26 cm and was immersed in water with a freestream velocity of 0.3 m/s. The plunging motion schedule was prescribed by a plunge-amplitude of 10.13 cm and frequency 0.1178 Hz. A C-mesh with 737 × 65 grid points was used for the pure plunging case, with a far-field set at 25 chords away from the airfoil. As in a previous study [10], 1,920 timesteps were used to discretize one plunge cycle. Figure 2 compares the computed lift coefficient obtained by the 2D OpenFOAM simulations with the previous 2D large-eddy simulations [10] and experiments [11]. Although there are some discrepancies between the results using two different motion functions, the current OpenFOAM simulations predicted the same trend of the lift coefficients when compared with the previous computed and experimental data. The discrepancies resulting from the two motion functions were mainly attributed to the round-offs when generating the motion schedule and calculating the grid speed, to which the transitional flow is sensitive.

3.3 NACA 0005 Airfoil in Pitch-Plunge Motion

To facilitate the ability for more complex multi-DOF motion schedules, the flow past a 2D NACA 0005 airfoil in pitch-plunging motion was simulated. The airfoil had a chord length of 64 mm and the freestream velocity was 63.5 mm/s with water as the fluid. The instantaneous position of the airfoil was expressed as a linear superposition of motion due to plunging (translation) and that due to pitching (rotation). The motion in both pitch and plunge was sinusoidal and the amplitudes were 48 mm and 30°, respectively. The airfoil pitched about its leading edge, which was consistent with a passively twisted wing of the type envisioned for flapping nano air vehicles. The pitching motion of the airfoil led the plunging motion by 90°. As with Ref. [12], the 2D calculations were performed on an O-type mesh with 481×129 grid points. The farfield boundaries were located about 25 chords away from the surface of the airfoil. The timestep was set to 3,840 per motion cycle.

Figure 3 compares the computed lift forces obtained by the 2D OpenFOAM laminar simulations with the previous CFD and experimental results [12], for a rectangular wing model (span, 25.4 cm) in water. In general there is good agreement between the computational and experimental results; for instance, there is repeatable behavior corresponding with the pitching-plunging motion schedule, the magnitudes of peak lift matched well, and there are no indications of obvious or significant phase shift. For the most part, the computed lift force fell within the uncertainty band of the measured lift force.

4 Validation of OpenFOAM Flow Solver for Ships in a Low-Sea State

Ref. [2] details the CFD development work which focuses on low-sea states, using the SFS2 to validate the pimpleFOAM for static cases, that is, cases where the ship is not in motion. After the validation, the methodology was applied to the CPF, which is a representative geometry, to generate the data used for flight simulator look-up tables. Some results from Ref. [2] are repeated here for completeness and to assist with the comprehension of the readers.

4.1 Model of Static Simple Frigate Shape

The static computations were performed first for a 1:100 scale model of the SFS2; this model was also tested experimentally in an NRC wind tunnel. A C-H type structured grid was used in this study. The farfield of the computational domain was set at $5l_s$ and the depth of the domain was set to $0.75l_s$, where l_s represents the total length of the ship. These parameters were determined based on previous ship airwake computational studies. The grid spacing in the ship airwake was uniform with 30.48 cm (1 ft) at full scale in all three directions. The mesh had approximately six million cells. The computations were performed for 346 units of flow through time (l_s/U_∞), with 330 used for spectral analysis.

Figure 4 compares the computed results with available experimental data for the head-

wind condition, including the mean pressure coefficient distribution on the SFS2 surfaces, mean longitudinal velocity at the hangar height on a mid-plane in the ship airwake over the flight deck, the corresponding turbulence intensities, and the power spectral density plots of the longitudinal velocity at a representative wake location. All of the trends measured in the wind tunnel data were generally replicated by CFD. The maximum discrepancy of the mean velocity between the current CFD and the experimental results is approximately 3%, which represents excellent agreement.

4.2 Static Canadian Patrol Frigate

With the successful validation of the CFD solver OpenFOAM against the SFS2 geometry, OpenFOAM was applied to the static CPF. Static testing of this ship has also been carried out in a wind tunnel at a scale of 1:50. Because the dimensions of some small structures are on the order of 3.8 mm (0.15 inches) for the full-scale CPF, the simulations were performed at full scale to keep the geometry and solution values at a reasonable magnitude that were greater than machine zero. Both the CFD and wind tunnel models included the masts and other smaller structures of the CPF. Owing to the complexity of some superstructure features, unstructured grids were used near the ship, except in the airwake where a structured grid was employed, as demonstrated in Figure 5. Figure 6 shows the computed pressure distribution. For the static CPF, particle image velocimetry (PIV) was used to measure the vertical plane-wise flow characteristics in the CPF airwake. Figure 7 illustrates the planes laid out over the CPF flight deck for the PIV measurements, with a slightly simpler mast. The PIV measurements were performed for the headwind and Red 20° (a wind coming from the portside) wind conditions. Since difficulties were initially encountered with meshing, instabilities, and high consumption of computational time, subsequent simulations were conducted without the masts. Figure 8 demonstrates comparisons of computed flow field with the PIV results. They are in good agreement, showing similar flowfield features and magnitudes. In addition, the computations also confirmed that the inclusion of the anemometer masts in the airwake simulations plays a secondary role when compared with the choice of numerical scheme [2].

5 Simulation of Airwake Flows behind the CPF in Motion

5.1 Wind Tunnel Measurements

Experimental investigations of the airwake flows behind the CPF in motion were conducted at the NRC 3 m × 6 m wind tunnel. Figure 9 shows the setup of the CPF model and the ship-motion system in the test section of the wind tunnel. Spires placed at the entrance of the test section created a simulation of the atmospheric boundary layer. The frigate model was a 1:50-scale above-water model of the CPF.

Measurements of velocity at discrete points in the ship airwake were acquired with four Cobra probes mounted on the flight deck. The layout of the Cobra probes for airwake measurements is illustrated in Figure 10. Three Cobra probes – starboard, centre, and port – were placed inline at a distance of 14 m at full scale from the hangar face. An additional Cobra probe was placed directly downstream of the centre probe. Five elevation configurations were investigated to survey the airwake representing full scale heights from 5.5 m to 9.5 m above the flight deck. The wind-tunnel airwake measurements were acquired at a sampling rate of 5,000 Hz, with a low-pass filter frequency of 1,505 Hz.

Sinusoidal ship-motion profiles were used to understand the basic effects of motion resulting from a parametric variation in the amplitude and frequency of the motions. Simple sinusoidal profiles consisted of motion for one-DOF only (heave, roll, or pitch). The motion frequency was 0.08 Hz at full scale. The amplitudes were 1.5 m for the heave, 3.4° for the pitch, and 5° for the roll conditions, respectively. Multi-DOF motions were measured as well, using combined sinusoidal profiles which consisted of motion for two- or three-DOF; realistic profiles were also developed by the Defence Research and

Development Canada (DRDC) using typical seaway characteristics.

5.2 CFD Simulations

Computations were performed for flows around the CPF in headwind and Red 15° wind conditions. This paper reports the results for simple and combined sinusoidal profiles, which were identical to those of the wind tunnel. The computations for realistic profiles are ongoing. The motion solvers used were the solid-body and the modified dynamic RBF solvers. The solid-body solver does not allow deforming free-surface boundaries, which may cause numerical inaccuracy but serves as an effective tool for concept-proving. Both oscillating and tabulated motion functions were used. The tabulated motion function allowed for simple scaling of the motion profiles from the wind tunnel tests, based on the reduced frequency, to match the full-scale CFD conditions. The computations produced a very large data set (on the order of terabytes). To prove the concept and demonstrate the capability, only the results computed using the solid-body solver with the single and combined sinusoidal profiles are compared against wind tunnel data in this paper. Detailed analysis of the other results, including those using the dynamic RBF solver with multi-DOF motions, will be discussed in a later journal publication.

5.3 Results and Discussion

Table 1 and Table 2 compare selected computed results against equivalent experimental data, in terms of the mean values of normalized flow velocity magnitude, pitch, and yaw, and their fluctuations. The computed results compared well to the experimental data in general, for both static and motion conditions. Both computational and experimental simulations confirm typical bluff-body aerodynamic airwake phenomena over the flight deck, as evidenced by higher-speed flows at starboard (probe 2) and portside (probe 4) but lower speed at the centre (probe 2), and decrease of the speed when the probe moved lower (not shown). Also not shown is that the turbulence or flow fluctuations increased as the probes moved lower in the airwake. In general, the CFD results showed less unsteadiness than the experimental results. With the exception of flow unsteadiness, which must be higher to achieve the appropriate level of fidelity, the level of agreement shown in Table 1 is consistent with the level of agreement desired. As the technology continues to evolve, the reasons for the differences are expected to be understood, and agreement may improve.

When compared against Table 1, Table 2 reveals that the ship motions intensified the flow fluctuations over the flight deck, in both magnitude and directions (pitch and yaw), with the strongest influence due to ship pitch motion. The relative discrepancy between CFD and wind tunnel data is not consistent, which may provide insight into the strengths and weaknesses of the different computational approaches under development. Table 2 also shows that oblique wind angles amplified the flow directional fluctuations in the airwake over the flight deck.

Figure 11 shows the difference in the spectra of the centre probe at the height of the rotor plane in helicopter high hover for three simple sinusoidal cases: heave, roll, and pitch. The flow speed spectra showed periodic response at the motion frequency. Pitch motion had the most significant impact on the airwake while heave has lesser and roll had minimal impact at headwinds conditions. Although the computed magnitude of the oscillations were higher, the current CFD predicted the similar trends comparable to the experimental ones, with lower overall energy which is consistent with the results in Table 1 and Table 2. It is believed, once we have more time series, the spectra will be more accurate.

6 Concluding Remarks

The open-source software OpenFOAM was validated for computations of unsteady incompressible flows past airfoils in one- and two-DOF motion. It was also applied for simulations of airwake flows for a ship undergoing various motion profiles. Applying the solid-body motion solver, which did not model the deforming free-surface boundary around the CPF, the computed results showed reasonable agreement

with the wind tunnel data, demonstrating the ability and potential of OpenFOAM's motion solvers and functions to capture important features in unsteady airwake flows when the ship is in motion. Further studies are required to improve the computational accuracy so that the CFD results can be used to support applications for representative ship motions. In particular, work to refine the RBFs to model the dynamic free-surface boundary movement is in progress.

7 Acknowledgments

The present work was partially funded by DRDC and the Defense Technologies and Sustainment (DTS) program of NRC. Dr. Chris Sideroff from the Applied CCM Canada provided technical support for porting the RBF motion functions.

References

[1] Yuan, W., Lee, R., and Wall, A. Simulation of Unsteady Ship Airwakes using OpenFOAM. *30th Congress of the International Council of the Aeronautical Sciences,* Daejeon, Korea, 25-30 September, 2016.

[2] Yuan, W., Wall, A., and Lee, R. Combined Numerical and Experimental Simulation of Unsteady Ship Airwakes. *Computers and Fluids*, Vol. 172, pp 29-53, 2018.

[3] Zan, S. On Aerodynamic Modelling and Simulation of the Dynamic Interface. *Proc Inst Mech Eng, Part G: J Aerospace Eng*, Vol. 219, No. 5, pp 393–410, 2005.

[4] Spalart, P.R., Deck, S., Shur, M.L., Squires, K.D., Strelets, M.K., and Travin, A. A New Version of Detached-eddy Simulation, Resistant to Ambiguous Grid Densities. *Theoretical and Computational Fluid Dynamics*, Vol. 20, No. 3, pp 181–195, 2006.

[5] OpenFOAM. The Open Source CFD Toolbox. *User Guide*, Version v1706, June 2017.

[6] Applied CCM Canada. *Caelus*. http://www.caelus-cml.com/, 2017.

[7] Bos, F. M., van Oudheusden, B. W., Bijl, H. Radial Basis Function Based Mesh Deformation Applied to Simulation of Flow Around Flapping Wings", *Computers & Fluids*, Vol. 79. pp 167–177, 2013.

[8] Halfman, R. L. *Experimental Aerodynamic Derivatives of a Sinusoidally Oscillating Airfoil in Two-Dimensional Flow*. NACA Report 1108, 1952.

[9] Yuan, W., Khalid, M. Computation of Unsteady Flows past Aircraft Wings at Low Reynolds Numbers. *Canadian Aeronautics and Space Journal*, Vol. 50, No. 4, pp 261-271, 2004.

[10] Yuan, W., Khalid, M. Flow Analysis of a Flapping SD7003 Airfoil at Transitional Reynolds Numbers. *27th AIAA Applied Aerodynamics Conference*, San Antonio, USA, June 22-25, AIAA-2009-3955, 2009.

[11] Ol, M., Bernal, L., Kang, C, and Wei, S. Shallow and Deep Dynamic Stall for Flapping Low Reynolds Number Airfoils. *Experiments and Fluids*, Vol. 46, pp 883-901, 2009.

[12] Yuan, W., Lee, R., Levasseur, L. Experimental and Computational Investigations of Flapping Wings for Nano Air Vehicles. *Engineering Applications of Computational Fluid Mechanics,* Vol. 9, No. 1, pp 199-219, 2015.

Copyright Statement

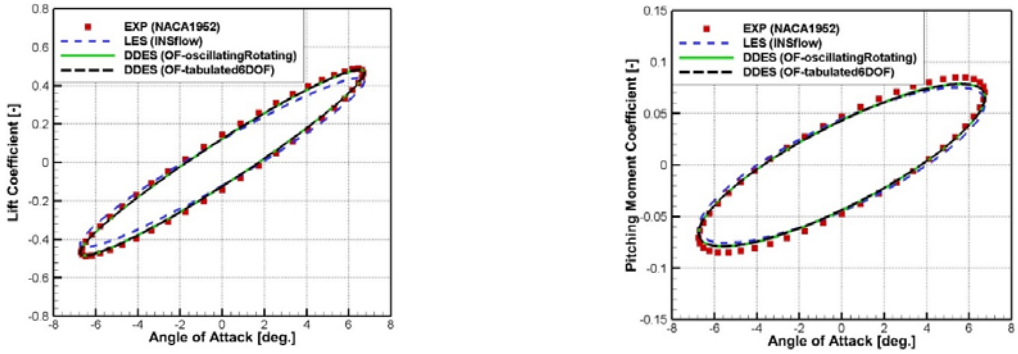

Figure 1. Lift (left) and pitching moment (right) coefficients for the NACA 0012 wing in pitching motion in air, $\theta = -6.74^{o}\sin(\omega t)$, $k_c = \omega c / 2u_\infty = 0.4$, $\mathrm{Re} = 6.9 \times 10^5$.

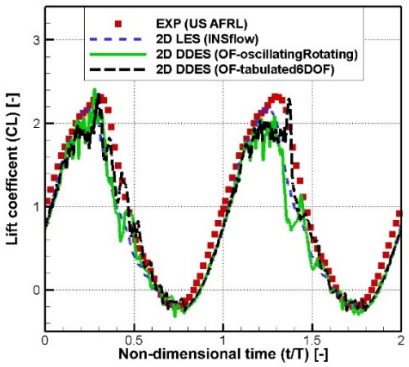

Figure 2. Lift coefficients of the SD7003 airfoil at $\mathrm{Re} = 6.0\times10^4$ in plunging motion $h(t) = H\sin(\omega t + 90°)$ with $f = 0.1178$ Hz in water.

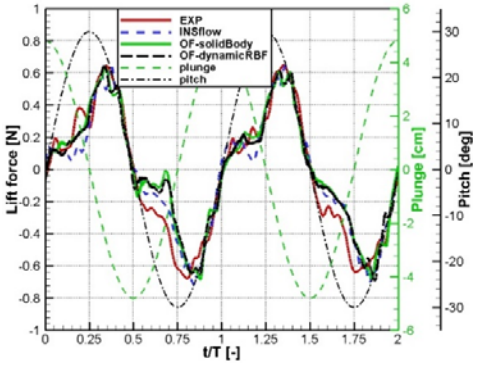

Figure 3. Computed and measured lift force for the pitching-plunging NACA 0005 airfoil at $\mathrm{Re} = 10.5 \times 10^3$, $U_\infty = 0.0635$ m/s in water, $f = 0.5$ Hz.

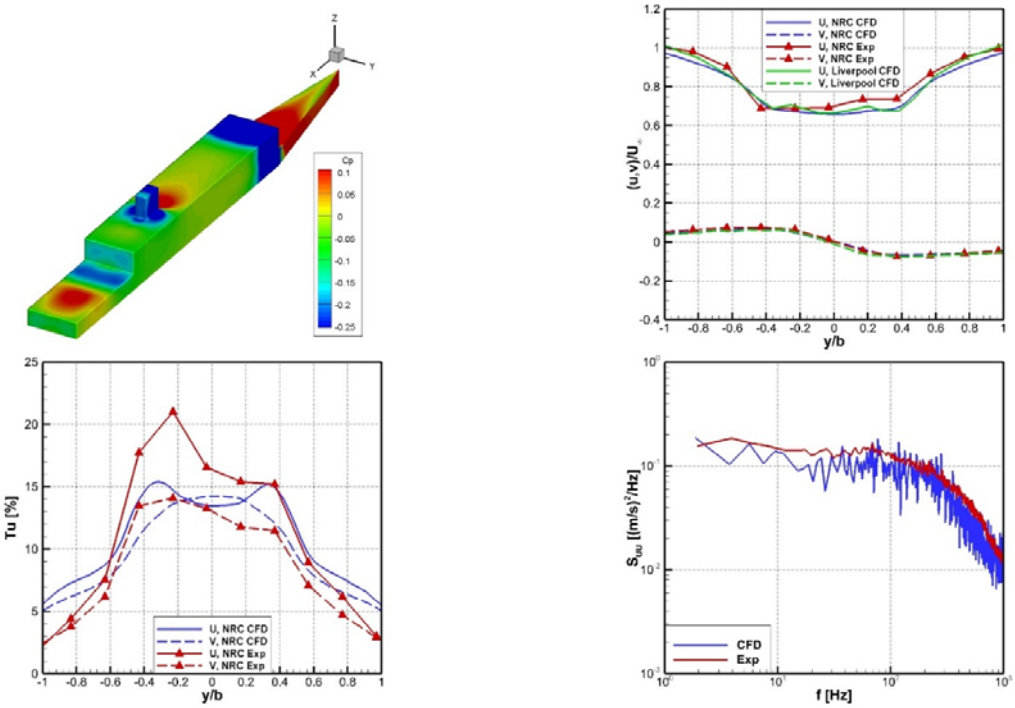

Figure 4. Computed results for the SFS 2 model at headwind condition.

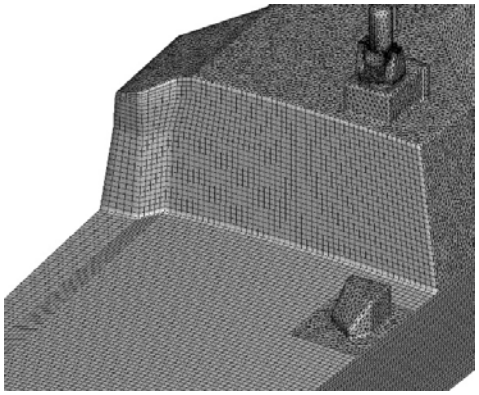

Figure 5. Surface mesh covering the CPF used in the CFD study.

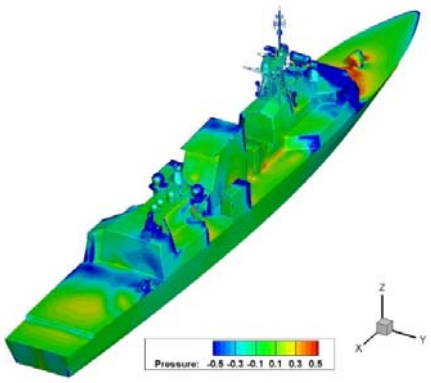

Figure 6. Computed pressure distribution on the CPF surfaces.

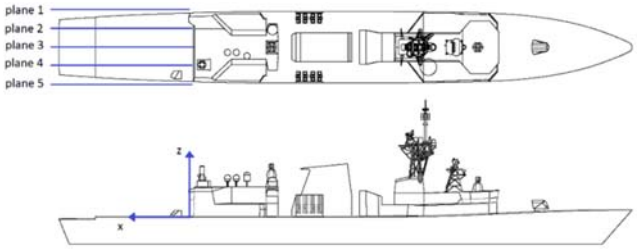

Figure 7. Layout of the PIV measurement planes located in the CPF ship airwake. Here, the model depicts a high-fidelity main mast.

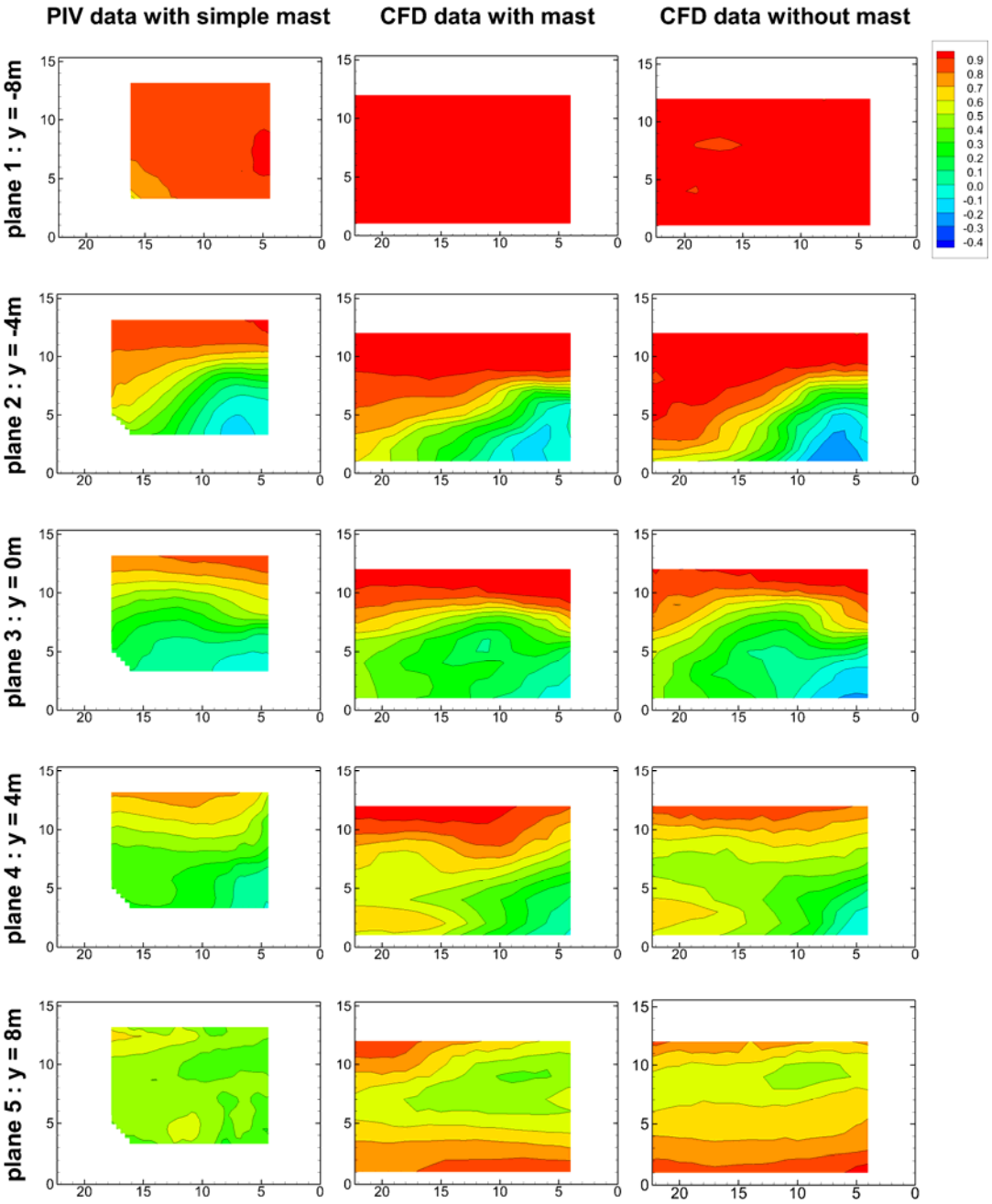

Figure 8. CPF airwake data, Red 20° wind, streamwise mean flow, dimensions in metres.

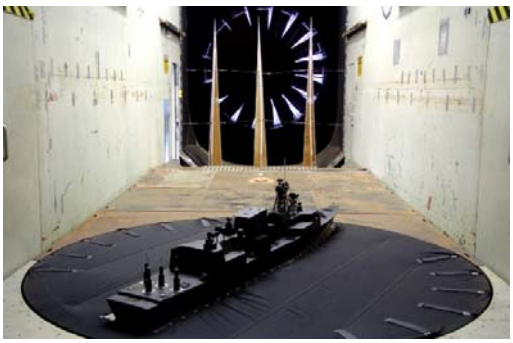

Figure 9. Setup of the oscillating CPF model in the wind tunnel.

Figure 10. An array of Cobra probes mounted on the flight deck of the oscillating CPF model.

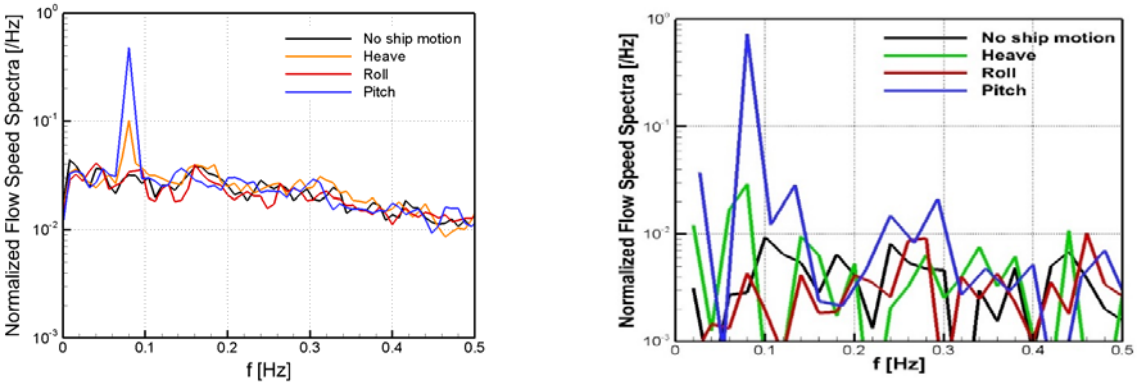

Experimental Computed

Figure 11. Effect of ship motion on airwake.

Table 1 Mean velocity magnitude (U/U_∞), pitch $\theta[°]$, and yaw $\psi[°]$, and fluctuations of velocity (U'/U_∞), pitch $\theta'[°]$, and yaw $\psi'[°]$ in the CPF flight deck wake at headwind condition, no motion

Probes	x[m]	y[m]	z[m]	U/U_∞		$\theta[°]$		$\psi[°]$		U'/U_∞		$\theta'[°]$		$\psi'[°]$	
				CFD	Exp	CFD	Exp	CFD	Exp	CFD	Exp	CFD	Exp	CFD	Exp
4	14	-5	9.5	0.89	0.89	-4.97	-8.03	3.18	0.16	0.10	0.14	3.83	6.91	4.34	9.03
3	14	0	9.5	0.76	0.76	-9.01	-8.66	0.41	-3.44	0.09	0.16	5.41	9.09	7.41	12.15
2	14	5	9.5	0.88	0.81	-6.23	-4.32	-4.15	-4.22	0.12	0.18	5.17	9.50	4.97	11.37
1	19	0	9.5	0.78	0.79	-7.98	-12.75	0.85	-2.13	0.08	0.15	4.68	8.01	6.62	11.03

Table 2 Mean velocity and fluctuations of velocity in the airwake over the flight deck behind the CPF in motion, at the highest elevation (z = 9.5 m) of the centre probe (x = 14 m)

Condition	Motion	U/U_∞		$\theta[°]$		$\psi[°]$		U'/U_∞		$\theta'[°]$		$\psi'[°]$	
		CFD	Exp	CFD	Exp	CFD	Exp	CFD	Exp	CFD	Exp	CFD	Exp
Headwind	Heave	0.77	0.76	-9.45	-8.66	0.26	-2.73	0.10	0.16	5.54	9.03	6.77	12.21
Headwind	Pitch	0.63	0.76	-11.07	-8.85	1.86	-2.61	0.23	0.17	10.61	9.08	12.93	12.06
Headwind	Roll	0.78	0.76	-9.83	-8.53	0.44	-2.41	0.09	0.15	4.75	8.86	8.01	12.00
Red 15°	Heave	0.79	0.84	1.88	-1.32	22.41	21.23	0.18	0.21	11.53	11.01	13.72	13.24
Headwind	Heave-Pitch	0.72	0.76	-9.77	-8.51	0.72	-2.78	0.15	0.16	6.38	9.16	8.31	12.24
Headwind	Heave-Roll	0.76	0.76	-9.29	-8.67	0.39	-3.32	0.11	0.16	5.99	9.23	7.76	12.36